ORIGINAL ARTICLE

Boundary currents in a meridional channel subject to seasonally varying buoyancy forcing: application to the Tsushima Current

Young Ho Seung · Kuk Jin Kim

Abstract The theoretical problem of formation of boundary currents in an idealized basin subject to seasonally varying buoyancy forcing is considered in an attempt to apply it to the seasonally varying Tsushima Current. Until now, all the theories intended to explain the branching of the Tsushima Current have been for the annual mean Tsushima Current—the seasonally varying Tsushima Current has never been properly explained. A simple numerical experiment shows that eastern and western boundary currents change in time, concurrently, when local buoyancy forcing is sufficient, as it is in the Tsushima Current. However, this is not true for ineffective local buoyancy forcing. The importance of the role played by local buoyancy forcing is further supported by simple theoretical considerations. Overall, this study suggests that effective local buoyancy forcing is probably essential to the formation of seasonally varying eastern and western boundary currents of the Tsushima Current.

Y. H. Seung (✉)
Department of Oceanography, Inha University,
Incheon 402-751, Korea
e-mail: seung@inha.ac.kr

K. J. Kim
Ocean Research and Strategy Corp, Seoul 153-760, Korea

1 Introduction

The problems of buoyancy-forced boundary currents in the presence of heat exchange with the atmosphere have been studied by Davey ([1983](#)) for a meridional channel and by Spall ([2003](#)) for a meridional island. In these studies, only steady buoyancy forcing is considered and the same problems with seasonally varying buoyancy forcing have not yet been studied. A good example of buoyancy-forced boundary currents forming along the eastern and western meridional boundaries can be found in the East/Japan Sea[1] (EJS[1]).

The EJS[1] is a marginal sea in the western North Pacific, with shallow openings connecting them, and is subject to strong buoyancy flux (Hirose et al. [1996](#)). Oceanic subtropical water enters the EJS[1], driven by the sea-level difference between the subtropical and sub-polar gyres (Minato and Kimura [1980](#); Ohshima [1994](#)), through the southern opening, called the Korea/Tsushima Strait, and flows out through the northern openings, the Tsugaru Strait and further north the Soya Strait, forming the Tsushima Current (Fig. [1](#)). Volume transport through the Tsugaru Strait is larger than that through the Soya Strait but is less seasonally variable (Nishida et al. [2003](#)). The region dominated by the water carried by the Tsushima Current is called the warm-water region. North of this region is a nearly isolated region, called the cold-water region, separated from the warm-water region by a sub-polar front. In the warm-water region, the Tsushima Current splits into two branches, one, called here the western boundary current, flowing along the western boundary and the other, called here the eastern boundary current, flowing along the

---

[1] The Editor-in-Chief recommends the usage of term "Sea of Japan" or "Japan Sea" in place of "East/Japan Sea".
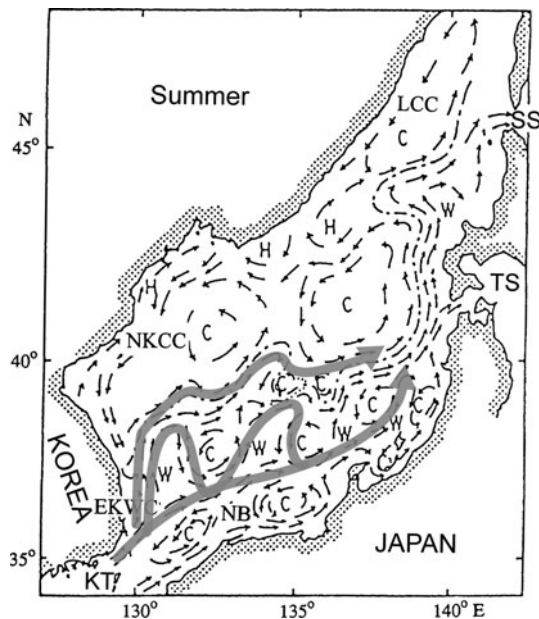
Fig. 1 Schematic diagram of surface circulation of the EJS[1] in summer (after Naganuma 1977; adapted from Kim and Yoon 1999). *LCC* Liman Cold Current, *NKCC* North Korean Cold Current, *EKWC* East Korean Warm Current, *NB* nearshore branch, *H* relatively high-temperature region, *C* cold-water region, *W* warm-water region, *SS* Soya Strait, *TS* Tsugaru Strait, *KT* Korea/Tsushima Strait. *Thick shaded arrows* indicate the eastern and western boundary currents of the Tsushima Current

southern and eastern boundaries. The former is usually called the East Korean Warm Current. It separates from the coast before reaching the latitude of outflow openings and then runs northeastward toward the outflow openings parallel to the sub-polar front. Part of the eastern boundary current is known to form a large meander and associated eddy, called the Ulleung Warm Eddy (Ichiye and Takano 1988), on entering the basin, before approaching the southern and eastern boundaries. Except for the current flowing close to the Japanese coast, called the Nearshore Branch, which is affected by bottom topography (Yoon 1982a), the eastern boundary current is usually called the Offshore Branch (Kawabe 1982a). The cold-water region is strongly affected by local wind forcing, which is very strong and variable because of orographic effects (Yoon and Kawamura 2002). In the warm-water region, however, current pattern depends greatly on volume transport through inflow opening, neither the western nor the eastern boundary current being formed by local wind forcing (Fig. 8 in Hogan and Hulbert 2000).

Theories attempting to explain the branching of the Tsushima Current have been proposed. Yoon (1982b) suggested that the western boundary current is because of the β-effect, i.e., westward propagation by Rossby waves of high-pressure disturbances associated with the positive buoyancy anomaly created further east. Kawabe (1982b)

explained that the Offshore Branch is a transient feature, appearing only in the summer season, associated with an increase of volume transport and propagating as coastally trapped waves. However, observations and most of the numerical experiments cited above show that the Offshore Branch is present even in winter and is very weak near the bottom, except for the Nearshore Branch, indicating that it is not affected by bottom topography. On the other hand, Spall (2002) emphasizes the effect of thermal damping (local buoyancy forcing) in the formation of the eastern boundary current. The buoyancy surplus carried by Kelvin waves from the inflow (southern) opening is rapidly distributed along the eastern boundary. Without thermal damping, it is spread westward by Rossby waves ultimately causing western intensification, the so-called β-effect. By thermal damping, however, it decays offshore creating the thermally induced eastern boundary layer. If this is true, the western boundary current should be created by a mechanism other than the western intensification proposed by Yoon (1982b). According to Spall (2002), this may be local wind forcing with negative stress curl, which, in fact, is proved by Hogan and Hulbert (2000) not to be true, as described above. Two more ideas suggest that the branching is caused by local effects, that is, without the β-effect: Cho and Kim (2000) considered that the branching is hydraulically triggered within the Korea/Tsushima Strait. On the other hand, Ou (2001) considered that it arises because of hydraulic control and bottom friction along the channel of the inflow opening.

The western and eastern boundary currents are known to undergo simultaneous seasonal variation, as observed by Morimoto and Yanagi (2001) and suggested by most numerical experiments (Seung and Yoon 1995; Kim and Yoon 1999; Kim 2008; Sasajima et al. 2007; Kawamura et al. 2009). Long-term measurements of volume transport performed in the Korea/Tsushima Strait (Fukudome et al. 2010) indicate that the western and eastern boundary currents are strongest in the fall, because the Tsushima Current is highly dependent on its volume transport. The theories mentioned above are all for the annual mean Tsushima Current and they do not adequately explain why the western and eastern boundary currents undergo simultaneous seasonal variation. Without local forcing, seasonal variation of the western boundary current is possible only if Rossby waves transfer westward the signals of seasonal variation occurring on the eastern boundary. The time taken by Rossby waves of speed βR^2 (R is the Rossby radius), of the order of 10^{-3} m s^{-1}, to cross the basin with zonal dimension of order 10^3 km is much longer than a year. Hence, simultaneous seasonal variation of the western and eastern boundary currents is apparently impossible. However, seasonally varying local buoyancy forcing may explain well the observed seasonal character of the

Tsushima Current, as it does for the annual mean Tsushima Current (Spall 2002). In this study, this will be shown to be true. First, a simple numerical experiment is performed for an idealized basin to show that properly designed seasonally varying buoyancy forcing can indeed lead to the eastern and western boundary currents, analogues of the western and eastern boundary currents of Tsushima Current, with simultaneous seasonal variation. Next, a further simplified analytical model is considered to gain insight into the dynamics of formation of seasonally varying boundary currents. Conclusions and discussion end the paper in the Sect. "4".

2 Numerical model

Assume that the ocean considered is active only in the upper layer overlying a deep motionless layer (Fig. 2). The buoyancy, or the pressure, can then be represented by the upper-layer thickness, $H + h$ where H is a reference value and h is the thickness anomaly from H. Next, consider a marginal sea idealizing the EJS[1] basin. The upper layer of the marginal sea communicates with that of the ocean through two narrow openings, one in the south and the other in the north (Fig. 3). The northern opening represents both the Tsugaru and the Soya Straits. Because of the pressure gradient orienting northward, oceanic subtropical water enters the marginal sea through the southern opening, flows along the eastern boundary, associated with Kelvin waves, and then radiates westward, associated with Rossby waves. The eastern boundary current thus formed can be compared with the Offshore Branch of the Tsushima Current. The portion of the marginal sea dominated by the subtropical water can be regarded as the warm-water region of the EJS[1]. The cold-water region is present north of the warm-water region, isolated from both the ocean and the warm-water region. On the large scale, where the Kelvin and Rossby waves play major roles in adjustment to buoyancy forcing, the idealized warm-water region can be regarded as equivalent to a basin embedded in a meridional channel between two reservoirs, one with oceanic subtropical water to the south and the other with the water of the cold-water region to the north (Fig. 3). In the real situation, the boundary between the warm-water and cold-water regions is not a straight line. We simply assume that the shape of boundary does not fundamentally change the dynamics of the large-scale current within the warm-water region (hereafter called "basin").

The basin is subject both to local buoyancy forcing and to the pressure gradient arising from the buoyancy difference. If the basin is isolated from the reservoirs, it will have buoyancy, referred to as "adjusted buoyancy", by adjusting itself to local buoyancy forcing. The oceanic subtropical
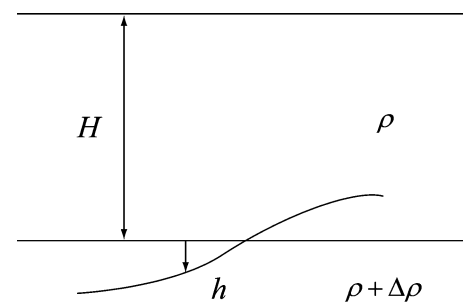

Fig. 2 Definition sketch, showing an active upper layer overlying a deep motionless lower layer. H is a reference value and h is the deviation from this
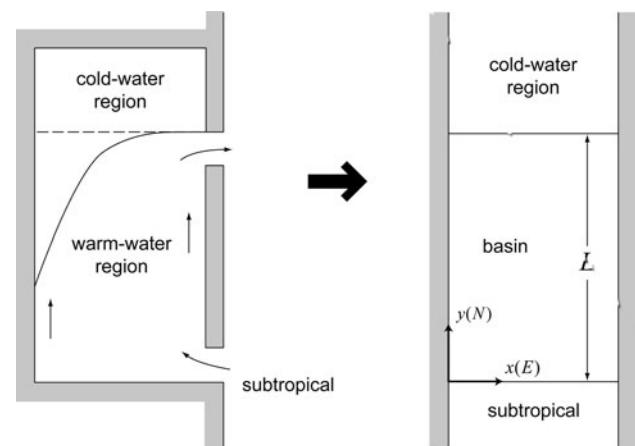

Fig. 3 *Left* Schematic diagram showing the marginal sea on the western side of the ocean. Oceanic subtropical water enters the marginal sea through the southern opening and flows out through the northern opening, forming a warm-water region. North of the warm-water region, a cold-water region is present, isolated from the ocean. *Thin arrows* denote currents. *Right* A basin embedded in a meridional channel between two reservoirs filled with oceanic subtropical water to the south and water of the cold-water region to the north. The *thick arrow* pointing to the right means that the situation shown on the left is dynamically equivalent to that shown on the right. The *X*- and *Y*-axes point, respectively, eastward (E) and northward (N) with their origin at the southwestern corner of the basin

water carried into the basin tends to have adjusted buoyancy as a result of the effect of local buoyancy forcing. The adjusted buoyancy in the basin is less than that of the oceanic subtropical water and larger than that of the water found in the cold-water region, decreasing northward within the basin.

Take H as the mean value of the upper-layer thickness in the northern reservoir. Let h_s and h_n be, respectively, the thickness anomaly in the southern and northern reservoirs, and let h_{in} be the thickness anomaly of the basin corresponding to the "adjusted buoyancy". The quantity h_{in} is assumed to decrease linearly with y. Because the difference between the thickness of the layers is the essential factor driving the motion, only the values of h_s and h_{in} measured relative to h_n will be taken into consideration, i.e., $h_n = 0$

is assumed. Because both h_s and h_{in} can be regarded as undergoing the same seasonal variation, i.e., change with time without any phase difference, they can be expressed as:

$$h_s = \Delta h\,[1 + r\sin\{2\pi(t - T/4)/T\}], \tag{1}$$

$$h_{in} = \{(2\alpha - 1)y/L + (1 - \alpha)\}h_s, \tag{2}$$

where Δh is the difference between the mean layer thickness in the southern and northern reservoirs, $r\Delta h$ $(0 < r < 1)$ is the amplitude of seasonal variation of h_s, $T = 1$ year is the period, t denotes the time measured from the time when both h_s and h_{in} are minimum (Fig. 4), y is the meridional distance measured from the southern boundary of the basin (c.f., Fig. 3), and α is a number $(0 < \alpha < 0.5)$ measuring the latitudinal change of h_{in}. In Eq. 1, r is taken such that h_s is usually positive. In Eq. 2, latitudinal change of h_{in}, $\partial h_{in}/\partial y$, depends on α, ranging from $\partial h_{in}/\partial y = 0$ for $\alpha = 0.5$ to $\partial h_{in}/\partial y = -h_s/L$ for $\alpha = 0$, with $h_{in} = 0.5h_s$ at $y = L/2$ in all cases. With β-plane approximation, the governing equations are:

$$\frac{\partial u}{\partial t} + u\frac{\partial u}{\partial x} + v\frac{\partial u}{\partial y} = (f_0 + \beta y)v - g'\frac{\partial h}{\partial x} + A\nabla^2 u, \tag{3}$$

$$\frac{\partial v}{\partial t} + u\frac{\partial v}{\partial x} + v\frac{\partial v}{\partial y} = -(f_0 + \beta y)u - g'\frac{\partial h}{\partial y} + A\nabla^2 v, \tag{4}$$

$$\frac{\partial h}{\partial t} + \frac{\partial}{\partial x}[(H + h)u] + \frac{\partial}{\partial y}[(H + h)v] = \frac{1}{\tau}(h_{in} - h), \tag{5}$$

where (u, v) are the (x, y)-components of the velocity, f_0 is the typical Coriolis frequency, β is the latitudinal gradient of the Coriolis frequency, g' is reduced gravity, A is the eddy viscosity, and τ is the time taken to restore h to h_{in}. In Eq. 5, the effect of local thermal forcing is represented by restoration of h to h_{in} with restoration time τ. When $h > h_{in}$, the upper layer thickness h decreases with time by warm-to-cold water mass conversion, and vice versa. This kind of buoyancy forcing is widely used (Spall 2002). For small τ, restoration is rapid, resulting in strong buoyancy forcing, and vice versa. Hence, the inverse of τ measures the effectiveness of local buoyancy forcing.

Numerical experiments were performed with Eqs. 3 through 5 and using the conditions expressed by Eqs. 1 and 2, using the early version of MICOM (Bleck and Boudra 1986). This model uses bi-harmonic type eddy viscosity with the viscosity coefficient proportional to the absolute value of the total deformation of the horizontal motion field (Bleck and Boudra 1981). Constants of proportionality, say μ, ranging from 0.04 to 0.4 are considered. Because the results obtained for $0.04 \le \mu \le 0.4$ are basically the same, we will show only the result for $\mu = 0.1$. The basin considered has dimensions 800 km by 800 km in the zonal and meridional directions. The southern and northern reservoirs
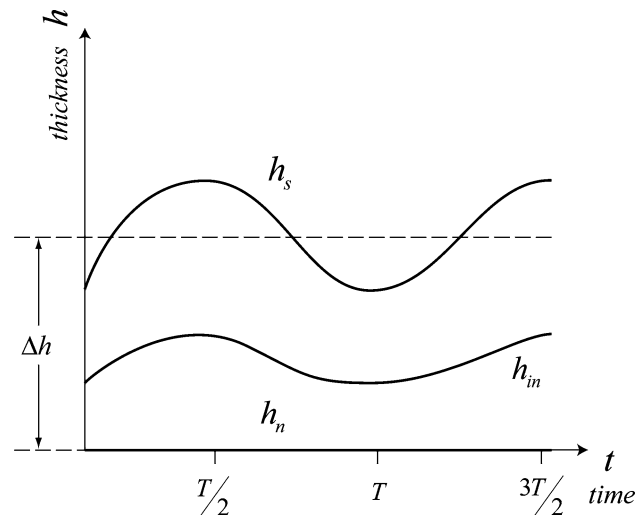

Fig. 4 Seasonal variation of upper-layer thickness in the southern reservoir, h_s, and that corresponding to the "adjusted buoyancy", h_{in}, at $y = L/2$. $t = 0$ corresponds to the time when both h_s and h_{in} are minimum. $T = 1$ year and both h_s and h_{in} are measured relative to the upper-layer thickness of the northern reservoir

have dimensions 400 km in the meridional direction and 800 km in the zonal direction. A square grid of size 10 km is used and the time-step is taken as $\Delta t = 720$ s. The values used are $H = 150$ m, $\Delta h = 30$ m, $f_0 = 10^{-4}$ s^{-1}, $\beta = 2 \times 10^{-11}$ s^{-1} m^{-1}, and $g' = 0.02$ m s^{-2}. The values of r and α are not known. Numerical experiments show that the general pattern of the boundary currents remains unchanged for the various r and α considered here; we use $r = 0.5$ and $\alpha = 0.25$. For effective local buoyancy forcing, oceanic response to atmospheric change may occur in less than a month, i.e., τ smaller than 30 days is considered as representing effective local buoyancy forcing. For the purpose of comparison, however, $\tau = 100$ days is also considered as an example of ineffective local buoyancy forcing.

The layer thickness in the northern reservoir is kept nearly constant at H by imposing a sufficiently strong restoration condition with restoration time linearly increasing from $\tau = \Delta t/100$ at the northern end of the reservoir to the values applied to the basin ($\tau = 10$, 30 and 100 days) at the boundary with the basin. In the same manner, the layer thickness in the southern reservoir is kept changing with time nearly the same as given in Eq. 1. Each reservoir is also treated as sponge layer, where motion is artificially damped by linear friction (not shown in Eqs. 3 and 4). The artificial damping coefficient decreases linearly from $100/\Delta t$ at the northern and southern ends of the reservoirs to zero at the boundaries with the basin; within the basin, motion is dissipated by eddy viscosity only. Time integration is performed for 11 years starting from $t = 0$ when h_s, and h_{in} are minimum; we refer $t = 0 + nT$

Fig. 5 Time series of potential and kinetic energies integrated over the basin for $\tau = 30$ days. Those for $\tau = 10$ days and $\tau = 100$ days (not shown) have the same patterns although the energy levels increase with τ. Time starts from the moment of minimum buoyancy
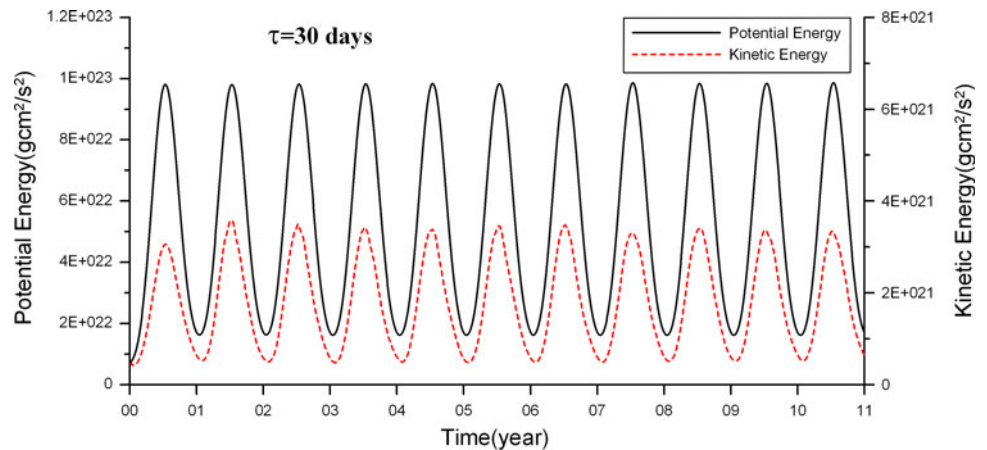
($n = 1$, 2,...) to minimum-buoyancy time and $t = 0.5T + nT$ ($n = 1, 2,...$) to maximum-buoyancy time. The results for the last year are used to obtain annual mean and seasonal means, the latter being obtained by averaging over 10 days around minimum-buoyancy or maximum-buoyancy time.

Time series of energy integrated over the basin indicate that seasonal variations are well reproduced (Fig. 5). To clarify the seasonal variation of the eastern and western boundary currents obtained by use of the model, distance–time diagrams are shown for $\tau = 10$ days, $\tau = 30$ days, and $\tau = 100$ days, where the distance is measured along the central zonal line located at $y = 800$ km (Fig. 6). For $\tau = 10$ days, cross-shore variation of the layer thickness, $\partial h / \partial x$ (>0), is largest (smallest) at the maximum-buoyancy time (minimum-buoyancy time) simultaneously on the western and eastern boundaries, indicating that eastern and western boundary currents undergo simultaneous seasonal variation, as they do in the EJS.[1] This can be confirmed for currents obtained around $t = 10T$ and $t = 10.5T$ (Figs. 7, 8). Note that the eastern boundary current around $t = 10T$ is almost invisible for $\tau = 30$ days compared with that for $\tau = 10$ days. The seasonal character of the boundary currents is quite different for $\tau = 100$ days (Fig. 6). Buoyancy signals represented by layer thickness propagate westward significantly far from the eastern boundary. As a result, it can happen near the minimum-buoyancy time that layer thickness increases offshore ($\partial h / \partial x < 0$) on the eastern boundary, leading to a southward current on eastern boundary with a northward counter current further offshore. Although the westward-propagating signals slowly decay with time as a result of local buoyancy forcing, the layer thickness on the western boundary is highly variable in time, indicating that the current is not always strongest (weakest) at maximum-buoyancy time (minimum-buoyancy time). In fact, model results obtained in the 11th year show that the current on the eastern boundary is southward around the minimum-

buoyancy time and that on the western boundary is not distinctively stronger in the maximum-buoyancy period than in the minimum-buoyancy period (Fig. 9). In annual mean current, the western and eastern boundary currents are well identifiable for effective local buoyancy forcing (for $\tau = 10$ days and $\tau = 30$ days) but the eastern boundary current is not quite distinctive for ineffective local buoyancy forcing (for $\tau = 100$ days) (Fig. 10).

For all the cases considered, the western boundary current extends further to the north than the western boundary current of the Tsushima Current does (Fig. 1). This discrepancy arises from the fact that the meridional dimension of the model basin is exaggerated compared with that of the warm-water region of the EJS[1]. A meander associated with an anti-cyclonic gyre is usually observed near the southwestern corner. This may be the high-pressure bulge usually formed by non-linear effects near the entrance where buoyant water debouches, similar to that obtained numerically by Yoon and Suginohara (1977). It may also be compared with the Ulleung Warm Eddy described earlier. However, its role in formation of boundary currents is not known. For the meridional buoyancy gradient considered above, and for τ ranging from 10 to 100 days, inflow and outflow transport are, respectively, approximately 1.2 and 1.0 Sverdrup. Hence, the rate of warm-to-cold water mass conversion by local buoyancy forcing is approximately 0.2 Sverdrup, although it decreases slightly with τ.

3 Dynamics of boundary current formation

To gain more physical insight into formation of the boundary current, the problem is further simplified by assuming that the magnitude of the motion induced by buoyancy forcing is infinitely small such that non-linear terms can be neglected, and eddy–viscosity dissipation is replaced by linear friction with coefficient k. A further
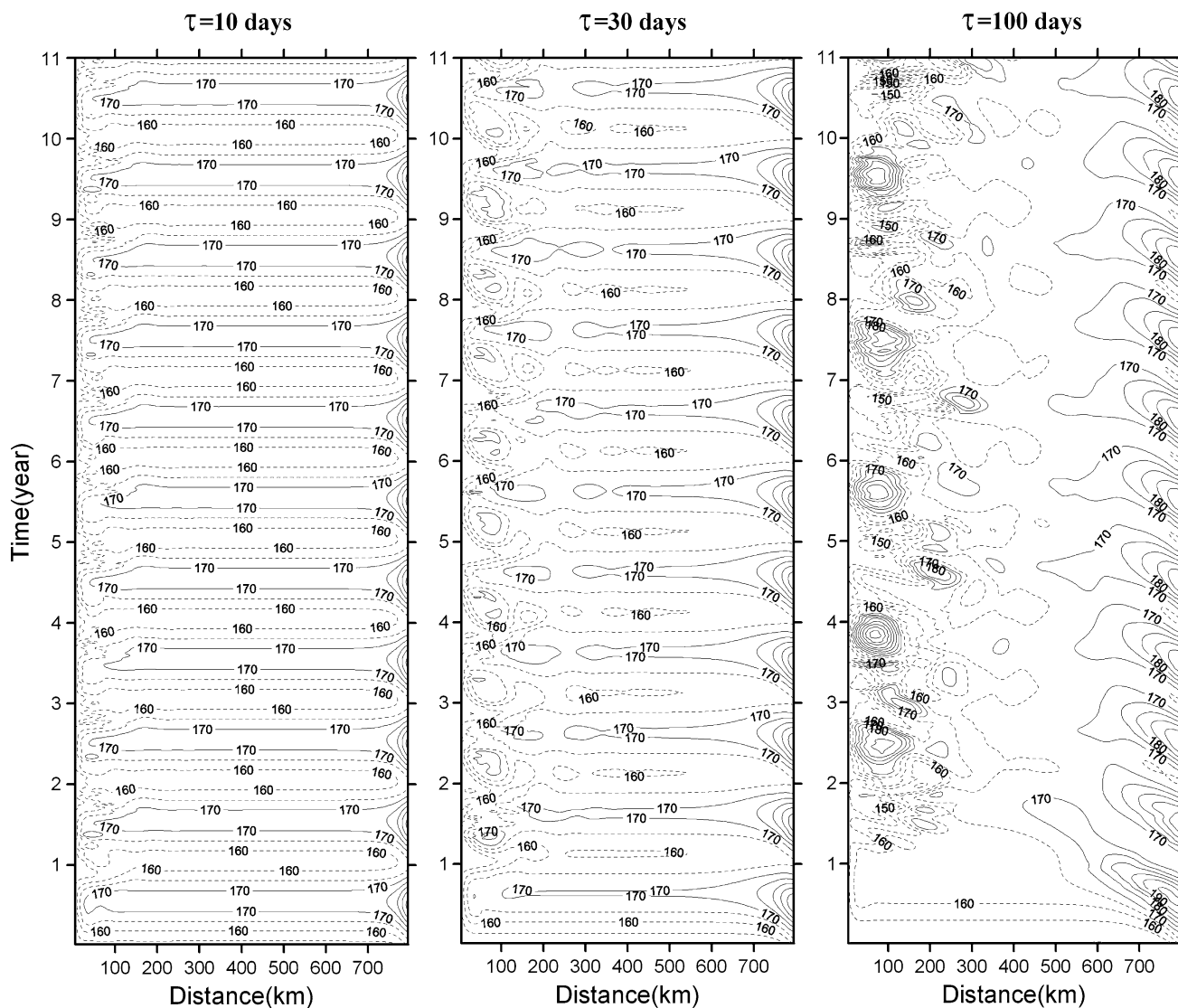
Fig. 6 Distance–time diagrams of upper-layer thickness for $\tau = 10$ days, $\tau = 30$ days, and $\tau = 100$ days. Distance is measured in the x-direction (eastward) along the line $y = 800$ km. Values equal to or larger than 170 m are in *solid lines* and those less than 170 m are in *dotted lines*. Time starts from the moment of minimum buoyancy

assumption is that the meridional component of current is largely geostrophic. This assumption is based on the fact that $u \ll v$ near the meridional boundaries, both u and v are very small and friction are negligible in the interior, and $T \gg 1/f$ ($T = 1$ year is the time scale of motion). Then, the governing equations are:

$$fv = g' \frac{\partial h}{\partial x}, \tag{6}$$

$$\frac{\partial v}{\partial t} = -fu - g' \frac{\partial h}{\partial y} - kv, \tag{7}$$

$$\frac{\partial h}{\partial t} + H\left(\frac{\partial u}{\partial x} + \frac{\partial v}{\partial y}\right) = (h_{in} - h)/\tau. \tag{8}$$

Cross-differentiation of Eqs. 6 and 7, using 8, leads to the following vorticity equation:

$$\frac{\partial}{\partial t}\left[\frac{\partial^2}{\partial x^2} - \frac{1}{R^2}\right]h = -\frac{1}{R^2\tau}(h_{in} - h) - \beta\frac{\partial h}{\partial x} - k\frac{\partial^2 h}{\partial x^2}, \tag{9}$$

where $R = \sqrt{g'H}/f_0$ is the Rossby radius. Applying the no-normal flow boundary condition $u = 0$ at $x = 0$ and at $x = L$ to Eq. 7 with use of Eq. 6 leads to:

$$\frac{\partial h}{\partial y} = -\left(\frac{1}{f_0}\frac{\partial}{\partial t} + \frac{k}{f_0}\right)\frac{\partial h}{\partial x} \ll \frac{\partial h}{\partial x}. \tag{10}$$

The magnitude of the terms within the parentheses is much smaller than unity because $T \gg 1/f_0$ and $f_0 \gg k$. Note that $1/f_0$ is less than 1 day and $1/k$ is considered to be a few tens of days, say $1/k = 30$ days. Hence, the no-normal boundary condition is found to be equivalent to negligible variation in the meridional direction compared

Fig. 7 Distribution of upper-layer thickness (in m) and current vector (in cm s^{-1}) averaged over the minimum-buoyancy and maximum-buoyancy periods for $\tau = 10$ days. Results for the last year are averaged over 10 days around $t = 10T$ and $t = 10.5T$ for, respectively, the minimum-buoyancy and maximum-buoyancy periods
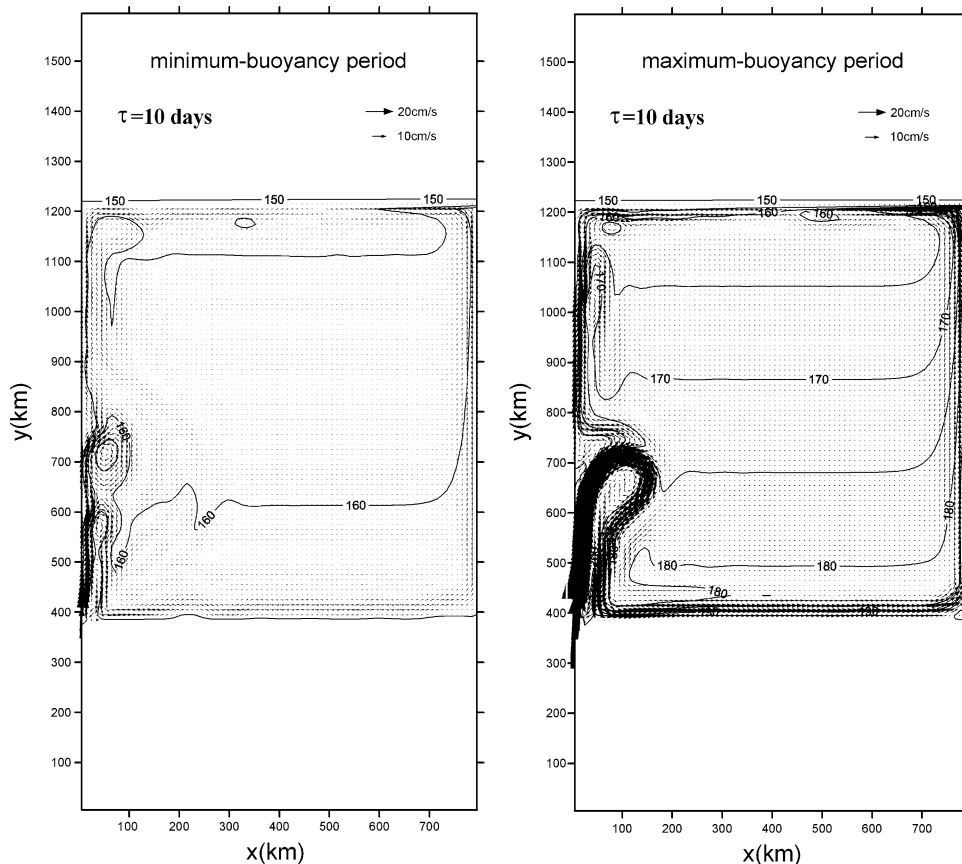
with that in zonal direction, and it suffices to consider only the zonal variation along a latitude line, e.g., the latitude line passing through the central region of the basin. Because $\partial h/\partial y \approx 0$, obtained above, and using Eqs. 1 and 2, boundary conditions for h can be written as:

$$h = h_n = 0 \quad at \quad x = 0, \tag{11}$$

$$h = h_s = \triangle h[1 + r\sin\{2\pi(t - T/4)/T\}] \quad at \; x = L, \tag{12}$$

which means that layer thickness along the eastern (western) boundary becomes immediately equal to that in the southern (northern) reservoir as a result of the effect of rapidly propagating Kelvin waves. The analytical solution is obtained by solving Eq. 9 with the conditions expressed by Eqs. 11 and 12. In what follows, two extreme cases are considered, one is for very ineffective local buoyancy forcing ($\tau = \infty$) and the other is for very effective local buoyancy forcing ($\tau \ll T$).

3.1 Very ineffective local buoyancy forcing ($\tau = \infty$)

In this case, the terms with τ on the right-hand side vanish. The layer-thickness anomaly (briefly, layer thickness) on the eastern boundary, varying in phase with that in the southern reservoir, propagates westward as long baroclinic

Rossby waves without undergoing thermal damping. On arriving at the western boundary, the Rossby waves are reflected, transformed into short Rossby waves and are rapidly dissipated by mechanical damping, leading to the formation of a Stommel boundary layer of width $L_s = k/\beta$. East of the Stommel boundary layer, the length scale of motion is of the same order as the zonal scale of the basin, L, which is much larger than both R and L_s. Note that the basin considered is characterized by $L = 800$ km, $R = 17$ km, and $L_s = 19$ km for the values used in the preceding section and for $k = 1/30$ days. The term with $\partial^2/\partial x^2$ on the left-hand side of Eq. 9 can thus be neglected compared with the term with R^2 to within the order of $(R/L)^2$. Likewise, the term with k on the right-hand side of Eq. 9 can be neglected compared with the term with β to within the order of L_s/L. The resulting governing equation is:
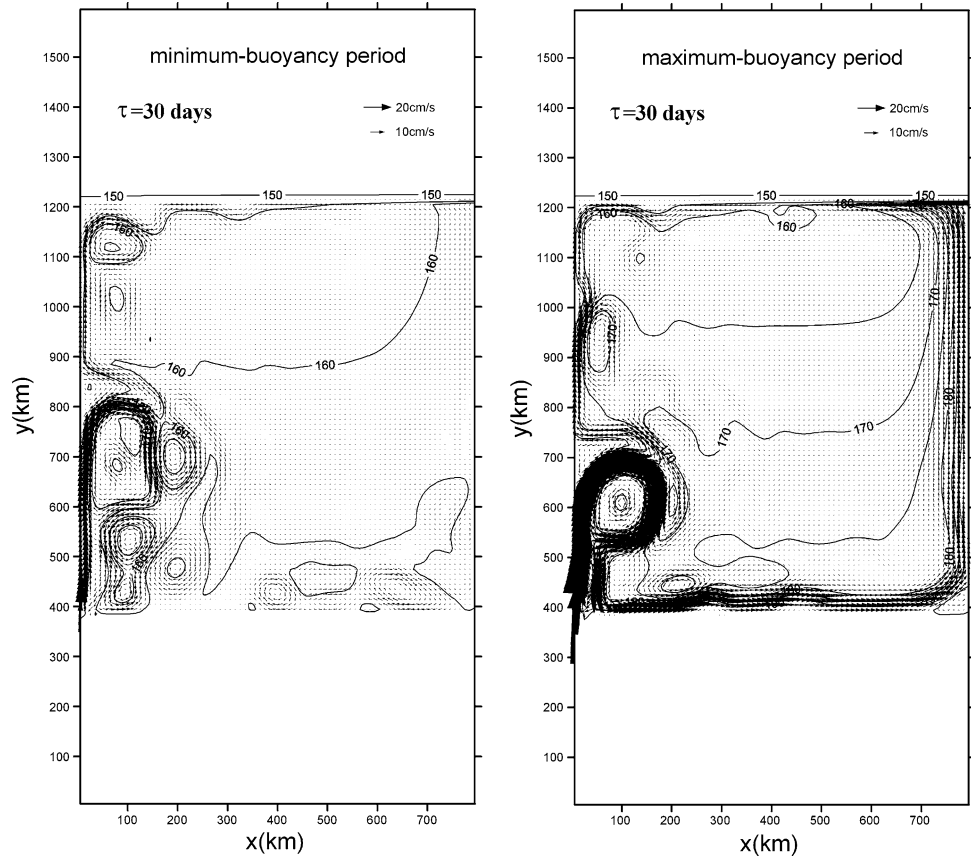
$$\frac{1}{R^2}\frac{\partial h}{\partial t} - \beta\frac{\partial h}{\partial x} = 0. \tag{13}$$

The solution to Eq. 13 satisfying Eq. 12 is:

$$h = \triangle h\left[1 + r\sin\left\{2\pi\left(t - \frac{T}{4} + \frac{x - L}{\beta R^2}\right)/T\right\}\right], \tag{14}$$

which implies that h imposed on the eastern boundary propagates westward with speed βR^2, the speed of long baroclinic Rossby waves. Hence, the current forming near

Fig. 8 Same as Fig. 7 except for $\tau = 30$ days

the eastern boundary is not always northward, being southward near the minimum-buoyancy time ($nT - T/4 < t < nT$; $n = 1, 2,\ldots$) when $\partial h/\partial x < 0$ at $x = L$ (Fig. 11).

Near the western boundary, boundary layer forms only by mechanical damping with length scale $L_s = k/\beta$, as noted above. Because $T \gg 1/k$, the term with $\partial^2/\partial x^2$ on the left-hand side of Eq. 9 can be neglected compared with the term with k on the right-hand side to within the order of $1/kT$ ($\ll 1$). The term with R^2 on the left-hand side is assumed to be smaller than the term with β on the right-hand side to within the order of $L_s/\beta R^2 T$ which is approximately 0.1 for the values given above. This means that L_s is much smaller than the distance traveled by long Rossby waves for 1 year. Hence, the validity of this assumption is marginal. Then, the resulting governing equation is:

$$\beta \frac{\partial h}{\partial x} + k \frac{\partial^2 h}{\partial x^2} = 0, \tag{15}$$

to within the order of $L_s/\beta R^2 T$. Because $L_s \ll L$, boundary layer approximation can be made. The corresponding interior condition can be obtained by introducing $x = 0$ to Eq. 14:

$$h = \triangle h\left[1 + r\sin\left\{2\pi\left(t - \frac{T}{4} - \frac{L}{\beta R^2}\right)/T\right\}\right] \tag{16}$$
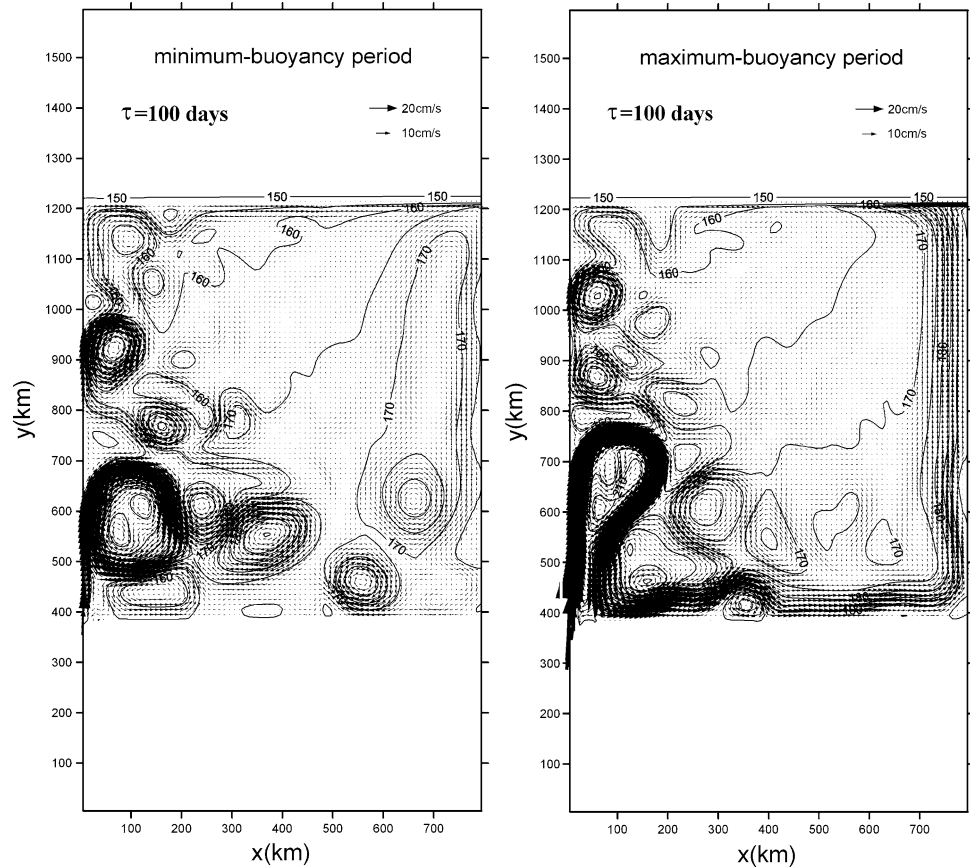
in basin interior.

The solution to Eq. 15 satisfying Eqs. 11 and 16 is:

$$h = \triangle h\left[1 + r\sin\left\{2\pi\left(t - \frac{T}{4} - \frac{L}{\beta R^2}\right)/T\right\}\right](1 - e^{-x/L_s}). \tag{17}$$

Because $\partial h/\partial x > 0$ at all times when $x = 0$, the northward western boundary current, with length scale $L_s = k/\beta$, always forms (Fig. 12). However, its phase is delayed by $2\pi L/\beta R^2 T$ relative to that of the buoyancy at $x = L$ given in Eq. 12. The value $L/\beta R^2 T$ is the ratio of the basin dimension to the distance traveled by the long Rossby waves for 1 year. For the values given above, $L/\beta R^2 T = 4.4$ corresponding to the time delay of 4.4 years (one can verify in Fig. 12 that signals of h_s appear 4.4 years later off the western boundary), which is too long for one to expect the western boundary current to change concurrently with the buoyancy on the eastern boundary—i.e., that the western boundary current is strongest (weakest) at maximum-buoyancy time (minimum-buoyancy time) cannot be expected.

Fig. 9 Same as Fig. 7 except for $\tau = 100$ days

3.2 Very effective local buoyancy forcing ($\tau \ll T$)

For very effective local buoyancy forcing, layer thickness propagating westward as Rossby waves is thermally damped rapidly and the basin interior adjusts to the local buoyancy forcing very quickly. Hence, the boundary layer forms near the eastern boundary and near the western boundary. The boundary layer width, say L_b, is not yet known but it is presumably much smaller than L, i.e., $L_b/L \ll 1$, as will shortly be evident. In the basin interior sufficiently far from the boundary layers, the basin rapidly adjusts to local buoyancy forcing and h is nearly the same as h_{in}. This can easily be shown by dimensional analysis of Eq. 9. In both the basin interior and the boundary layers, the term with R^2 on the left-hand side of Eq. 9 can be neglected compared with the terms with τ on the right-hand side to within the order of τ/T, and the term with $\partial^2/\partial x^2$ on the left-hand side can be neglected compared with the term with k on the right-hand side to within the order of $1/kT$. Hence, the terms on the left-hand side can be neglected over the whole basin. In the basin interior, the length scale is L, which is much larger than both R and L_b. Then, the term with $\partial^2/\partial x^2$ on the right-hand side can be neglected compared with the term with β to within the order of L_b/L. The term with β can also be neglected compared with the term with τ to within the order of L_τ/L, where $L_\tau = \beta R^2 \tau$ is

the distance traveled by long baroclinic Rossby waves for the period τ. Note that $L_\tau/L \ll \beta R^2 T/L$, by assumption, and that $\beta R^2 T/L = 1/4.4$ has already been obtained above. Hence, it is proved that $h = h_{in}$ in the basin interior:

$$h = h_{in} \quad \text{in basin interior.} \tag{18}$$

Within the boundary layers, the left-hand side of Eq. 9 can be neglected, as already shown above. The resulting governing equation for each boundary layer is:

$$k\frac{\partial^2 h}{\partial x^2} + \beta\frac{\partial h}{\partial x} + \frac{h_{in} - h}{R^2 \tau} = 0. \tag{19}$$

For boundary layer width much smaller than L, the boundary layer approximation can be made with the corresponding interior condition given in Eq. 18.

Equation 19 with the conditions expressed by Eqs. 11, 12, and 18 gives two solutions. One is for the eastern boundary layer and the other is for the western boundary layer. The solution for the eastern boundary layer is:

$$h = h_{in} + (h_s - h_{in})e^{(x-L)/L_E}, \tag{20}$$

where

$$L_E = L_s/2(-1 + \sqrt{1 + 4L_s/L_\tau}) \tag{21}$$

is the eastern boundary layer width. Equation 20 says that $h = h_s$ on the eastern boundary and exponentially
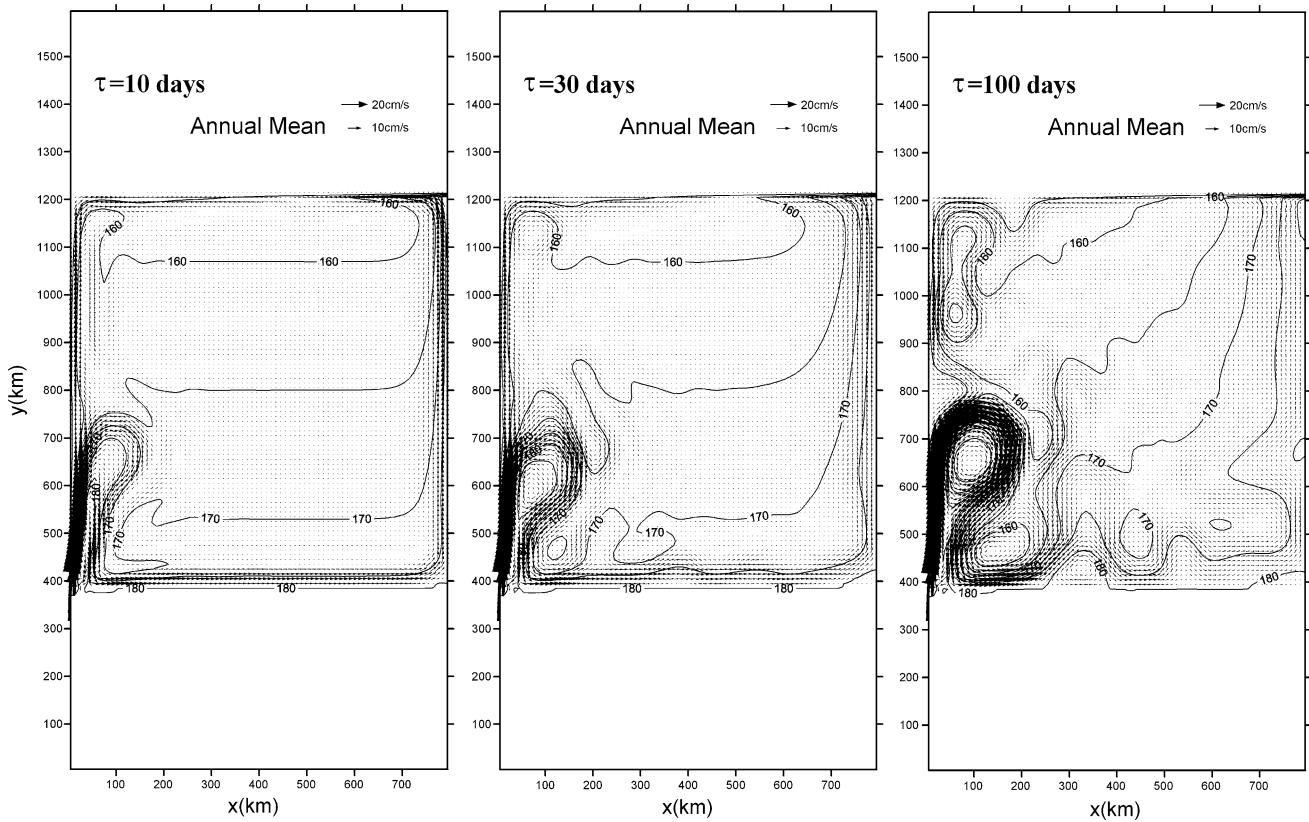
Fig. 10 Distribution of the annual mean upper-layer thickness (in m) and current vector (in cm s^{-1}) for $\tau = 10$ days, $\tau = 30$ days, and $\tau = 100$ days. Results for 11th year are averaged
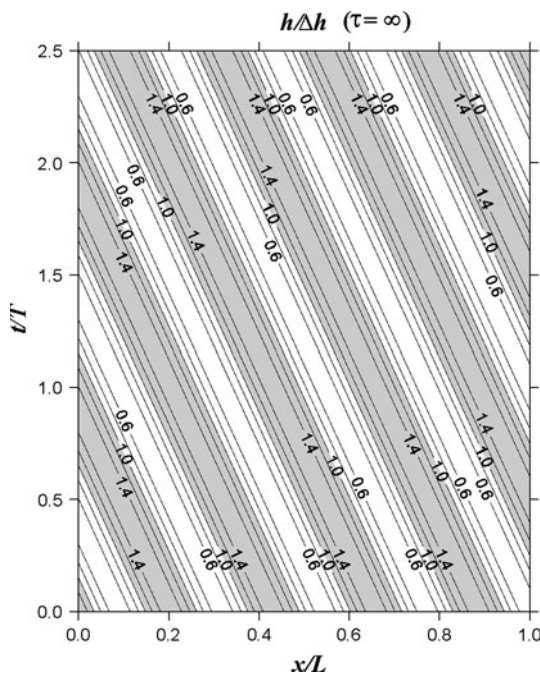

Fig. 11 Space-time diagram obtained by use of Eq. 14, showing westward propagation of $h/\Delta h$ from the eastern boundary $x/L = 1.0$, for $r = 0.5$ and $L/\beta R^2 T = 4.4$. Regions larger than 1.0 are *shaded*. Signals departing from $x/L = 1.0$ take more than 2.5 years to arrive at $x/L = 0$

decreases offshore to $h = h_{in}$ with length scale L_E. The solution for the western boundary layer is

$$h = h_{in}(1 - e^{-x/L_w}), \tag{22}$$

where

$$L_w = L_s/2(1 + \sqrt{1 + 4L_s/L_\tau}) \tag{23}$$

is the western boundary layer width. Equation 22 says that $h = 0$ on the western boundary and exponentially increases offshore to $h = h_{in}$ with length scale L_w. In Eqs. 21 and 23, the boundary layer widths depend on the value L_s/L_τ. L_W is smaller than L_s for all L_s/L_τ and L_E is smaller than L_s for $L_s/L_\tau > 0.3$, both becoming vanishingly small as L_s/L_τ goes to infinity. For the values given above, $L_s/L_\tau > 1$ if τ is less than 39 days as assumed here. Hence, the assumption $L_b/L \ll 1$ made earlier is proved to be valid. In Eqs. 20 and 22, $\partial h/\partial x > 0$ for all x and t, being maximum at $t = T/2 + nT$ ($n = 0, 1, 2, \ldots$), and minimum at $t = 0 + nT$ ($n = 0, 1, 2, \ldots$). It can be said that for sufficiently effective local buoyancy forcing, northward boundary currents always form on the western and eastern boundaries, being simultaneously strongest (weakest) at the maximum-buoyancy time (minimum-buoyancy time) (Fig. 13).

4 Concluding remarks

A theoretical problem of formation of boundary currents in an idealized basin subject to seasonally varying buoyancy forcing is considered in an attempt to understand the seasonally varying Tsushima Current. In the EJS[1], two

Fig. 12 Space–time diagram obtained by use of Eq. 17, showing the cross-shore distribution of $h/\Delta h$ near the western boundary, for $r = 0.5$ and $L/\beta R^2 T = 4.4$. Regions larger than 1.0 are *shaded*. The quantity $h/\Delta h$ increases offshore from $h/\Delta h = 0$ at $x/L_s = 0$ (western boundary) approaching the time-varying $h/\Delta h$ with length scale L_s

branches of the Tsushima Current, the northward-flowing western and eastern boundary currents, are known to undergo simultaneous seasonal variation. Until now, all the theories attempting to explain the branching of the Tsushima Current have been for the annual mean Tsushima Current, and not appropriate for the seasonally varying Tsushima Current. The model basin considered is bounded to the south and north by large reservoirs filled with water with buoyancy, respectively, larger and smaller than that of the water within the basin. In the basin, motion is driven by the buoyancy difference between the two reservoirs, and the basin tends to adjust to local buoyancy forcing. In these circumstances, a simple numerical experiment shows that eastern and western boundary currents undergo simultaneous seasonal variation for effective local buoyancy forcing, as they are in the Tsushima Current. However, this is not the case when the local buoyancy forcing is ineffective. Simple theoretical consideration gives physical insight into the formation of seasonally varying eastern and western boundary currents. For ineffective local buoyancy forcing, the buoyancy surplus distributed rapidly by Kelvin waves along the eastern boundary, changing seasonally, propagates westward as Rossby waves without significant thermal damping. Hence, current on the eastern boundary is not always northward, being southward when buoyancy is minimum on the eastern boundary. On the western boundary, the boundary current formed by mechanical damping does not change concurrently with buoyancy on the eastern boundary, because it takes too much time for
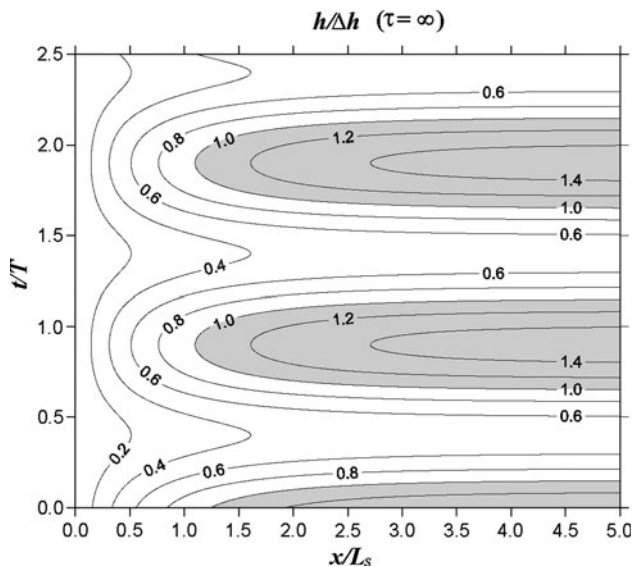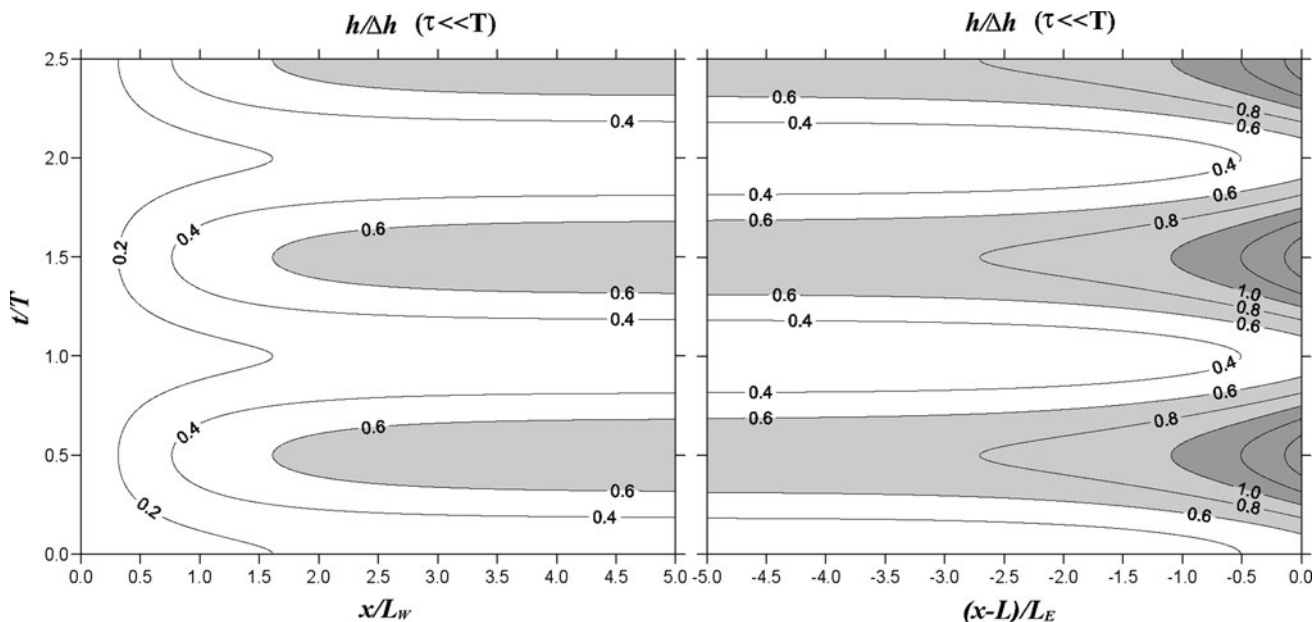

Fig. 13 Space–time diagram along $y = L/2$ obtained by use of Eqs. 20 and 22, showing cross-shore distribution of $h/\Delta h$ near the western (*left*) and eastern (*right*) boundaries, for $r = 0.5$ and $L/\beta R^2 T = 4.4$. x is measured negatively from the eastern boundary. The interior region, $x/L_W > 5.0$ and $(x - L)/L_E < -5.0$, is omitted because of the zonal uniformity of $h/\Delta h$. Regions larger than 0.6 and 1.0 are *shaded* separately. The same annual variation is observed for both the eastern and western boundary layers

long baroclinic Rossby waves, carrying buoyancy from the eastern boundary, to arrive at the western boundary. For effective local buoyancy forcing, however, the Rossby waves are thermally damped just off the eastern boundary, leading to the formation of the thermally driven eastern boundary layer and the subsequent eastern boundary current strongest (weakest) at the maximum-buoyancy time (minimum-buoyancy time). The western boundary is always dominated by less buoyant water, because of the Kelvin waves propagating from the north. Meanwhile, the basin interior gains buoyancy sufficiently fast as a result of local buoyancy forcing, largest (smallest) at the maximum-buoyancy time (minimum-buoyancy time), leading to formation of the western boundary layer and the subsequent northward western boundary current strongest (weakest) at the maximum-buoyancy time (minimum-buoyancy time). Hence, seasonally varying local buoyancy forcing is essential to the formation of the eastern and western boundary currents, both of which change seasonally.

According to Fukudome et al. (2010), volume transport of the Tsushima Current is maximum in the fall, not in the summer when the "adjusted buoyancy" is believed to be largest. We believe this discrepancy may arise from local effects, for example the typhoon passages usually occurring in this area (Moon et al. 2009). This model is based on large-scale dynamics and ignores local effects, for example that mentioned above. Throughout the paper, it is assumed that the eastern boundary current is not bottom-trapped. Because this assumption is not yet definitive, one may argue that the eastern boundary current is bottom-trapped. In this case, the buoyancy carried along the eastern boundary by coastally trapped waves, largest (smallest) at the maximum-buoyancy time (minimum-buoyancy time), cannot radiate westward effectively because it is topographically trapped, leading to the creation of the eastern boundary current offshore from the coastal buoyant water. For the western boundary current to be strongest (weakest) at the maximum-buoyancy time (minimum-buoyancy time), concurrently changing effective local buoyancy forcing is necessary in the same manner as it is when there is no topographic effect. Hence, the importance of local buoyancy forcing emerges again. Over all, this study reveals the importance of local buoyancy forcing in the formation of seasonally varying eastern and western boundary currents in a basin embedded in a meridional channel. Although this study is highly idealized, it suggests that effective local buoyancy forcing is essential to the formation of the western boundary current, and probably the eastern boundary current also, of the Tsushima Current.

References

Bleck R, Boudra DB (1981) Initial testing of a numerical ocean circulation model using a hybrid (quasi-isopycnic) vertical coordinate. J Phys Oceanogr 11:755–770

Bleck R, Boudra DB (1986) Wind-driven spin-up in eddy-resolving ocean models formulated in isopycnic and isobaric coordinates. J Geophys Res 91:7611–7621

Cho YK, Kim K (2000) Branching mechanism of the Tsushima Current in the Korea Strait. J Phys Oceanogr 30:2788–2797

Davey MK (1983) A two-level model of a thermally forced ocean basin. J Phys Oceanogr 13:169–190

Fukudome KI, Yoon JH, Ostrovskii A, Takikawa T, Han IS (2010) Seasonal volume transport variation in the Tsushima Warm Current through the Tsushima Straits from 10 years of ADCP observations. J Oceanogr 66:539–551

Hirose N, Kim CH, Yoon JH (1996) Heat budget in the Japan Sea. J Oceanogr 55:217–235

Hogan PJ, Hulbert HE (2000) Impact of upper ocean-topographical coupling and isopycnal outcropping in Japan/East Sea models with 1/8 degree to 1/64 degree resolution. J Phys Oceanogr 30:2535–2561

Ichiye T, Takano K (1988) Mesoscale eddies in the Sea of Japan. La Mer 26:69–79

Kawabe M (1982a) Branching of the Tsushima Current in the Japan Sea. Part I: data analysis. J Oceanogr Soc Jpn 38:95–107

Kawabe M (1982b) Branching of the Tsushima Current in the Japan Sea. Part II: numerical experiment. J Oceanogr Soc Jpn 38:183–192

Kawamura H, Ito T, Hirose N, Takikawa T, Yoon JH (2009) Modeling of the branches of the Tsushima Warm Current in the Eastern Japan Sea. J Oceanogr 65:439–454

Kim YJ (2008) A study on the Japan/East Sea oceanic circulation using an ultra-high resolution model. Dissertation, Kyushu University

Kim CH, Yoon JH (1999) A numerical modeling of the upper and the intermediate layer circulation in the East Sea. J Oceanogr 55:327–345

Minato S, Kimura R (1980) Volume transport of the western boundary current penetrating into a marginal sea. J Oceanogr Soc Japan 36:185–195

Moon JH, Hirose N, Yoon JH, Pang IC (2009) Effect of the along-strait wind on the volume transport through the Tsushima/Korea Strait in September. J Oceanogr 65:17–29

Morimoto A, Yanagi T (2001) Variability of sea surface circulation in the Japan Sea. J Oceanogr 57:1–13

Naganuma K (1977) The oceanographic fluctuations in the Japan Sea. Mar Sci 9:137–141 (in Japanese, with English abstract)

Nishida Y, Kanomata I, Tanaka I, Sato S, Takahashi S, Matsubara H (2003) Seasonal and interannual variations of the volume transport through the Tsugaru Strait. Oceanogr Jpn 12:487–499 (in Japanese, with English abstract)

Ohshima KI (1994) The flow system in the Japan Sea caused by a sea level difference through shallow straits. J Geophys Res 99:9925–9940

Ou HW (2001) A model of buoyant throughflow: with application to branching of the Tsushima Current. J Phys Oceanogr 31:115–126

Sasajima Y, Nakada S, Hirose N, Yoon JH (2007) Structure of the subsurface counter current beneath the Tsushima Warm Current simulated by an ocean general circulation model. J Oceanogr 63:913–926

Seung YH, Yoon JH (1995) Robust diagnostic modeling of the Japan Sea circulation. J Oceanogr 51:421–440

Spall MA (2002) Wind- and buoyancy-forced upper ocean circulation in two-strait marginal sea with application to the Japan/East Sea. J Geophys Res 107(C1). doi:10.1029/2001JC0009666

Spall MA (2003) Islands in zonal flow. J Phys Oceanogr 33:2689–2701

Yoon JH (1982a) Numerical experiment on the circulation in the Japan Sea. Part III. Mechanism of the Nearshore Branch of the Tsushima Current. J Oceanogr Soc Jpn 38:125–130

Yoon JH (1982b) Numerical experiment on the circulation in the Japan Sea. Part I. Formation of the East Korean Warm Current. J Oceanogr Soc Japan 38:43–51

Yoon JH, Kawamura H (2002) The formation and circulation of the intermediate water in the Japan Sea. J Oceanogr 58:197–211

Yoon JH, Suginohara N (1977) Behavior of warm water flowing into a cold ocean. J Oceanogr Soc Japan 33:272–282